Received: 12 April 2019 | Revised: 22 May 2019 | Accepted: 11 June 2019

DOI: 10.1002/htj.21528

HEAT TRANSFER
Asian Research

WILEY

ORIGINAL ARTICLE

Comparative analysis of nanofluid-based Organic Rankine Cycle through thermoeconomic optimization

Parth P. Prajapati | **Vivek K. Patel**

Department of Mechanical Engineering, Pandit Deendayal Petroleum University, Gandhinagar, Gujarat, India

Correspondence
Vivek K. Patel, Department of Mechanical Engineering, Pandit Deendayal Petroleum University, Gujarat, 382007, India.
Email: viveksaparia@gmail.com

Abstract

The present work focused on the comparative analysis of organic Rankine cycle (ORC) operated with nanoparticles. The effect of CuO and Al_2O_3 nanoparticles synthesized with water and circulated within heat exchangers are examined. Thermal efficiency and levelized energy cost (LEC) of the nanofluid based ORC are evaluated simultaneously in the present work. The optimization problem of ORC is formed and solved using heat transfer search algorithm. Operating parameters of the nanofluid based ORC such as pinch point temperature difference of heat exchangers, evaporation pressure, the mass flow rate of refrigerant, and concentration of nanoparticles are investigated in the optimization study. Further, the effect of turbine ratio, heat source temperature, and mass flow rate of heat source fluid on CuO and Al_2O_3 based ORC is explored and discussed. It was observed that a total variation of 35.2% was obtained at the cost of 3.5% variation in LEC between extreme design points. The maximum thermal efficiency of 19.3% and 19.32% can be obtained with CuO and Al_2O_3 with 2.616 and 2.62 $/kWh, respectively. Comparative results reveal that CuO based ORC shows dominance in terms of economic performance over Al_2O_3 based ORC for any given value of the thermal efficiency.

KEYWORDS

levelized energy cost, nanofluid, thermal efficiency, thermo-economic, waste heat recovery

1 | INTRODUCTION

To recover waste heat energy, Organic Rankine Cycle (ORC) has proven to be one of the promising technology for converting low-grade thermal energy into high-grade electric energy. Simple construction, ease of operation and maintenance and higher potential to recover waste heat energy compared to other methods, ORC is been focused upon by many researchers from the last two decades.[1] Extensive research has been done to enhance the performance of ORC with the aim of achieving higher efficiency.[2,3]

Experiments and simulation have shown that average thermal efficiency usually varies from 2% to 11% for small scale systems lesser than 5 kW.[4-7] ORC efficiency depends on multiple parameters like manufactured components, working fluid, operating parameters, types of the heat source and heat sink.[8] One of the important parameters for better operation of ORC is a selection of working fluids and many researchers have proposed models to select the fluid based on the application.[9] Liu et al[10] showed that wet fluids are inappropriate for the ORC technology as fluid will get converted to liquid vapor mixture and deteriorate turbine blades at the end of expansion. Similarly, Hung et al[6] examined the performance of the ORC system with wet, dry and concluded that isentropic fluids are ideal and considered to be the best among all available fluids.[11] In support of Hung's study, Imran et al[8] found that organic fluid R245fa is optimum working fluid for basic ORC because of very low investment cost and nonharmful characteristics.

Cost is a major factor for feasibility and commercialization of the project and depending upon the size of the plant, cost optimization has been a major area of focus for researchers. Much experimental work has been done on the small scale ORC models and very less work is reported for larger scales. Hajabdollahi et al[12] performed thermo-economic optimization for four different working fluids and they concluded that fluid R123 and R245fa has the highest thermal efficiency with the lowest cost. They could achieve a thermal efficiency of 51% at the lowest cost of 86,253 \$/kW. In one of his studies, Wang et al[13] achieved maximum exergy efficiency of 13.98% and a minimum total investment of 1.293×10^6 USD when ORC was operated at 403.15 K, 1.2 bar, and mass flow rate of 15 kg/s of exhaust gases. Scardigno et al[14] obtained the highest thermal efficiency of 9.65% using R134a as the working fluid with a minimum levelized energy cost of 0.114 \$/kWh using 363.15 K and 1 kg/s of water. On a larger scale, Fu et al[15] developed an ORC system of 250 kW with an axial turbine and working on R245fa. They achieved a net power output of 225 kW with a thermal efficiency of 7.94%. Han et al[16] built an ORC system of 200 kW working with double stage radial turbine using R245fa as working fluid. They could achieve a maximum of 201.2 kW with the heat source temperature of 144.1°C.

Scientists and researchers have been looking for methods to improve heat transfer and numerous materials are considered as alternative options for enhancement of heat transfer.[17-21] Metals and metal oxides, semiconductor materials, carbon nanotube, graphene, and so on. are used to enhance heat transfer. Selection of nanofluid usually depends on the thermo-physical properties of the material.[22,23] To determine thermophysical properties of nanofluids, various empirical models have been proposed but majorly they have failed to validate through experimental data. Nanofluids are prepared by mixing solid particles into base liquids such as alcohols, oils, water and so on, and it has been observed that major challenge during the synthesis of the nanoparticles is agglomeration.[24] For any nanofluid, thermal conductivity, viscosity, density, and specific heat are the most important thermo-physical properties which have to be investigated. Nallusamy[25] showed that the thermal conductivity ratio increases with an increase in particle volume fraction and his study were in good agreement with results reported in.[26]

Heat transfer coefficient of heat exchangers operated with nanofluids is higher than operated with conventional fluids.[27-29] For a shell and tube heat exchanger, an experiment was conducted by Farajollahi et al[30] by dispersing Al_2O_3 and TiO_2 with water and it was observed that TiO_2/water showed better heat transfer for lower concentrations whereas Al_2O_3/water mixture works better for concentrations higher at 0.3 v/v%. Wang et al[31] measured viscosity of Al_2O_3 water and Al_2O_3 ethylene glycol nanofluids and results showed that with an increase in the concentration of nanoparticles viscosity increases. Nallusamy[32] concluded that dispersion of Al_2O_3 nanoparticles in the water increases the thermal conductivity and viscosity of the Nanofluid and with an increase in particle concentration, this augmentation increases. Pak and Choi's[33] experiment supports that densities of Al_2O_3 and TiO_2 nanofluids get improved by 14% and 16%, respectively, as in when added to water at 25°C. With an increase in the concentration of nanoparticles, it can be observed that specific heats of the nanofluids mixture Al_2O_3/water, CuO/water, and SiO_2/water reduce but eventually increases with increase in temperature.[34]

Many researchers have been doing parametric optimization of the basic ORC and modified ORC for low-grade waste heat recovery.[9,35-38] Eventually researchers started using evolutionary algorithms to optimize multi-objective problems. Wang et al[39] carried out multiobjective optimization (MOO) using nondominated sorted genetic algorithm-II (NSGA-II) for condenser with the objective of minimizing heat transfer area and pressure drop using R134a.[39] Zhang et al[40] studied that R245ca is the most cost-effective during a thermo-economic study with the shortest static investment payback period among six potential dry organic fluids. Artificial Cooperative Search (ACS) algorithm was used by Turgut et al[41] to optimize specific investment cost (SIC) and second law efficiency of basic and single stage ORC using 12 different fluids. Feng et al[42] used Non dominated sorted genetic algorithm II for MOO of exergy efficiency and LEC for low-grade ORC using R245fa, pentane and their mixtures. To the best of authors knowledge majority of the research is done in multi-objective optimization of the ORC using various evolutionary algorithms using conventional heat transfer fluids. This work intends to add nanoparticles to the source fluid and it is circulated within heat exchangers to recover maximum thermal energy and heat transfer search algorithm is used to analyze the performance.

This work deals with the study showing the importance and benefits of using nanoparticles in the base fluid in the heat exchangers to enhance heat transfer. CuO and Al_2O_3 are considered for the study and comparative analysis is done to examine thermo-economic performance. Importance of pinch point temperature difference in evaporator and condenser, evaporation pressure, the mass flow of refrigerants and concentration of the nanoparticles have been studied and their effect on the objective function to minimize levelized energy cost and maximize thermal efficiency is discussed. Optimization is carried out using a multi objective heat transfer search algorithm. Refrigerant R245fa is used for the system analysis because of his nonharmful effect on the environment. It has very low toxicity, low ozone depleting potential and low flammability which makes it ideal fluid for the study. This work will help to understand the effect of nanofluids on heat transfer between the source fluid and working fluid to maximize thermal efficiency with minimum LEC.

Paper is organized in the following manner. ORC system is described in Section 2 along with a thermodynamic and economic model for nanofluid based ORC. Heat transfer search algorithm used to optimize the model is described in Section 3. Section 4 presents an application example of the considered ORC system and includes results and discussion. Investigation and study of the work is concluded in section 5.

2 | SYSTEM DESCRIPTION AND THERMOECONOMIC MODELING

Hot gases ORC is waste heat recovery technique used to utilize waste heat energy from the flue gases and converting it into useful power. It differs from a conventional Rankine cycle as ORC uses the organic fluid as its working fluid which has low boiling point temperature and can be superheated even at low temperatures. Source fluid relatively at a lower temperature than conventional Rankine cycle is used to convert organic fluid into superheated vapors. Heat transfer in evaporator takes place at constant pressure although certain irreversibilites in the system cause a pressure drop in the working fluid. Superheated vapor is expanded in a turbine and isentropic expansion of the working fluid will convert thermal energy of the organic fluid to mechanical energy of the turbine shaft which eventually is connected to the generator shaft. Low pressure, low temperature working fluid is then condensed in a condenser wherein water at a low temperature usually extracted from the natural water source is used to absorb the latent heat and condenses working fluid back to the liquid form. Organic fluid coming out to the condenser is pumped to the evaporator pressure using a pump wherein it again absorbs heat energy from the source fluid and it gets converted to superheated vapor and the cycle continues. Schematic diagram of the system and T-S diagram is shown in Figure 1 and Figure 2.

2.1 | Thermal model

Basic equations and correlations used in the investigation are presented in this section. Thermodynamic properties of nanofluids mixture is calculated by well-established models suggested by researchers. Among many properties, thermal conductivity, viscosity, density, and specific heat of the nanofluid are important properties which are determined using proven models. Shell and tube heat exchangers are used as evaporator and condenser for heat transfer between source fluid and working fluid. Heat transfer area of the heat exchangers and levelized energy cost is determined for

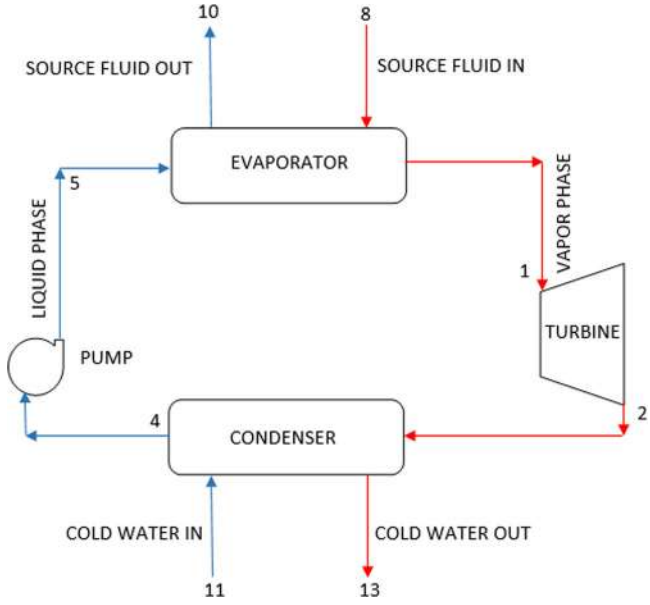

FIGURE 1 System layout of organic Rankine cycle [Color figure can be viewed at wileyonlinelibrary.com]

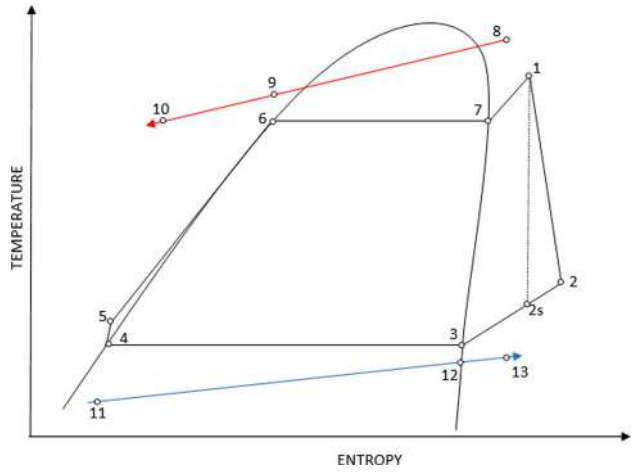

FIGURE 2 T-S diagram of ORC system. ORC, organic Rankine cycle [Color figure can be viewed at wileyonlinelibrary.com]

the system giving the insights of its thermal performance based on the maximum energy recovery. Correlations used in the analysis were taken from references.[33,43-49]

Thermal conductivity is one of the major thermophysical properties which denotes the capacity of any material to conduct heat. Thermal conductivity for liquids can be easily determined using Fourier's heat conduction principle. For nanofluid, there are many models developed which depends on multiple factors like particle volume concentration, temperature, particle size, particle shape, pH, and many more.[50] For this work, it is calculated using the equation suggested by Leong et al[47] as there is a prominent effect of particle size and interfacial layer on the conductivity of nanofluid.

$$K_{eff} = \frac{(K_{np} - K_l)\varnothing K_l[2\beta_1^3 - \beta^3 + 1] + (K_{np} + 2K_l)\beta_1^3[\varnothing\beta^3(K_l - K_f) + K_f}{\beta_1^3(K_{np} + 2K_l) - (K_{np} - K_l)\varnothing[\beta_1^3 + \beta^3 - 1]} \quad (1)$$

In Equation (1), β and β_1 are constants which depends on the ratio of interfacial layer thickness and particle radius ($\gamma = h/a$). Their values are given as $\beta = 1 + \gamma$ and $\beta_1 = 1 + \gamma/2$. For the current study, the particle radius is taken as 20 nm and interfacial layer thickness as 1 nm.

The density of nanofluids is determined as given by Gherasim,[51]

$$\rho_{nf} = (1 - \varnothing)\rho_f + \varnothing\rho_{np} \quad (2)$$

Brinkmans[38] correlation is used to determine the viscosity of nanofluids.

$$\mu_{nf} = \mu_{bf}(1 - \varnothing)^{-2.5} \quad (3)$$

Specific heat of nanofluid signifies heat capacities of solid and liquid phases when they are in thermal equilibrium. Xuan[49] proposed a correlation for calculating specific heats of nanofluids,

$$C_{p,nf} = \frac{(1 - \varnothing)\rho_f C_{p,f} + \varnothing\rho_p C_{p,np}}{\rho_{nf}} \quad (4)$$

TABLE 1 Properties of nanoparticles

Material	Thermal conductivity W/m.K	Density kg/m^3	Viscosity Pa·s	Specific heat J/kg·K
Water	0.6072	997.04	8.94×10^{-4}	4183
Al_2O_3	40	3900	...	880
CuO	33	6400	...	530

Thermodynamic properties of nanoparticles are listed in Table 1.

2.1.1 | Shell side calculations

The organic fluid is pumped at a higher pressure and fed to the evaporator wherein it absorbs heat energy from the source fluid. During heat transfer, working fluid gets converted to vapor phase and it occupies more volume inside the heat exchanger. Hence it is circulated within the shell side of the heat exchanger. Crossflow area for shell side, A_{cs}, and equivalent diameter D_e, is calculated using Equations (5) and (7),

$$A_{cs} = (D_s - N_t d_o)B \tag{5}$$

$$N_t = \frac{D_s}{P_t} \tag{6}$$

$$D_e = \frac{4\left(p_t^2 - \frac{\pi {d_o}^2}{4}\right)}{\pi d_o} \tag{7}$$

The dimensionless Reynolds number and Prandtl number for the refrigerant can be determined using Equations. (8) and (9).

$$Re_f = \left(\frac{\dot{m}_f}{A_{cs}}\right)\frac{D_e}{\mu_f} \tag{8}$$

$$\mathrm{P}_{rf} = \frac{C_{p,f} \times \mu_f}{K_f} \tag{9}$$

Nusselt number is expressed in terms of Reynolds number and Prandtl number which can be estimated as Equation (10),

$$Nu = 0.0266 \times \mathrm{Re}_f^{0.85} \times \mathrm{Pr}_f^{0.333} \tag{10}$$

Heat transfer coefficient of refrigerant is calculated in terms of Nusselt's number which is given as,

$$h = \frac{Nu \text{ x } k}{D_e} \tag{11}$$

2.1.2 | Tube side calculations

Nanoparticles synthesized with water is circulated within the tubes of shell and tube heat exchanger. Based upon the concentration of the nanoparticles added, mass flow rate of nanofluids is varied and determined. Weight of the nanofluids is calculated by,

$$W_{\mathrm{nf}} = \left(\frac{\varnothing}{100 - \varnothing}\right)\left(\frac{\rho_{np}}{\rho_{bf}}\right)W_{bf} \tag{12}$$

Cross sectional flow area of the tube is given by,

$$A_{o,t} = \frac{\pi}{4} d_i^2 N_{t,p} \tag{13}$$

The dimensionless Reynolds number and Prandtl number is calculated for tube side. Moreover, Nusselt number and heat transfer coefficient for turbulent flow is calculated as,

$$Nu = 0.024 \times \mathrm{Re}_{nf}^{0.8} \times \mathrm{Pr}_{nf}^{0.4} \tag{14}$$

$$h = \frac{Nu \times k}{d_i} \tag{15}$$

Thermal performance of heat exchanger is expressed in terms of overall heat transfer coefficient which is determined using the following Equation:

$$\frac{1}{U_o} = \frac{1}{h_{fS}} + \frac{d_o \ln\left(\frac{d_o}{d_i}\right)}{2K_w} + \frac{1}{h_{fT}}\frac{d_o}{d_i} \tag{16}$$

2.1.3 | Pumping power

With an increase in the concentration of nanoparticles in the base fluid, viscosity increases, and results in increased pumping power. For turbulent flow friction factor is determined by,

$$F = (0.790 \ln \mathrm{Re}_{nf} - 1.64)^{-2} \tag{17}$$

Mean velocity of nanofluids is expressed as,

$$\mathrm{U_m} = \frac{4\dot{m}_{\mathrm{nf}}}{\rho_{\mathrm{nf}} \pi d_{\mathrm{i}}^2} \tag{18}$$

Nanoparticles have a higher density as compared to the base fluid. Hence upon agglomeration, a viscosity of the mixture is bound to increase and eventually increase in pressure drop will be observed. Also, pumping power will increase with an increase in pressure drop of fluid within the heat exchanger. Pressure drop and pumping power is given by,

$$\Delta p = \frac{F\rho_{nf} U_m^2 L}{2d_i} \tag{19}$$

$$P = \dot{V}_{nf} \times \Delta p \tag{20}$$

2.1.4 | Heat transfer surface area

Size of the heat exchanger is determined by heat transfer surface area and heat duty. Heat transfer between source fluid and working fluid are obtained by,

Superheated region for evaporator,

$$Q_{sp} = m_f(h_2 - h_3) = m_w(h_{13} - h_{12}) \tag{21}$$

Two phase condensation region for condenser,

$$Q_{tp} = m_f(h_3 - h_4) = m_w(h_{12} - h_{11}) \tag{22}$$

Efficient heat transfer between two fluids in a heat exchanger is defined by a term called as pinch point temperature difference (PPTD). It is defined at a point where the minimum temperature difference between two fluids is observed. As shown in Figure 2, the difference between temperatures at point 6 and 9 for the evaporator is minimum whereas it is minimum between points 3 and 12 for the condenser. Smaller values of PPTD signifies efficient heat transfer between the fluids and a higher amount of energy can be recovered. Similarly higher PPTD signifies poor heat transfer between the source fluid and the working fluid. To enhance heat transfer in any heat exchanger it is recommended to keep minimum possible PPTD but it eventually increases cost of the heat exchanger. Moreover, it is expected that good design of heat exchanger will minimize the heat loss to the surrounding and should have minimum pressure drop within the tubes.

$$\Delta\text{PPTD}_{\text{eva}} = T_9 - T_6 \tag{23}$$

$$\Delta\text{PPTD}_{\text{cond}} = T_3 - T_{12} \tag{24}$$

Based on the pinch point temperature difference in the heat exchangers, temperatures of the source fluid and working fluid is determined and logarithmic mean temperature difference (LMTD) is determined which is represented as,

$$\text{LMTD} = \frac{\Delta T_{\max} - \Delta T_{\min}}{ln\frac{\Delta T_{\max}}{\Delta T_{\min}}} \tag{25}$$

Total heat transfer surface area of the heat exchanger is estimated by the following Equation:

$$A_{HX} = \frac{Q_t}{U_o \times \text{LMTD}} \tag{26}$$

Heat transfer surface area of the heat exchanger has a significant effect on the total cost of the system and accounts to the majority of the investment in the system. Hence it is of utmost importance to optimize the system for maximum thermal efficiency with a minimum area of heat exchangers.

One of the objective function for the current work is the thermal efficiency of the system which is given by Equation (27). The system should work with maximum possible thermal efficiency with a minimum amount of total investment.

$$\eta_{th} = \frac{W_t - W_p}{Q_{in}} \tag{27}$$

2.2 | Economic model

ORC works on the concept of waste energy recovery and it is of utmost importance that the system developed to recover energy should be installed and operated with minimum investment. To identify the performance of the system on economic grounds, levelized energy cost (LEC) is selected as another objective function with the aim of minimizing it. The total cost of individual components is calculated from using chemical engineering plant cost index for the year 2017.

The bare module of cost of the component is calculated using the following Equation:

$$C_{bm,X} = C_{p,X} F_{bm,X} \tag{28}$$

Where, $F_{bm,x}$ is bare module cost factor which is based on equipment material and working pressures. Values of $F_{bm,x}$ are specified in and listed in Table 2. $C_{p,x}$ denotes purchase cost which is given by the following Equation:

$$logC_{p,X} = K_{1,X} + K_{2,X}\, logY + K_{3,X}(logY^2) \tag{29}$$

In Equation (29), X is applicable for the type of equipment, that is, heat exchanger, turbine, and pump whereas Y specifies heat transfer through a heat exchanger or power capacities of turbine and pump. Values of component cost coefficients for K_1, K_2, and K_3 are given in Table 2. The total capital cost of the system can be calculated using the following Equation:

$$C_t = \sum C_{bm,X} \tag{30}$$

Considering the inflation rates of the market, the total cost of the system is calculated using cost index for the year 2017 and 2001 which is 623.5 and 397. The expression for a total cost of all the components is given as,

TABLE 2 Coefficients of the economic model

X	Y	Unit	$K_{1,x}$	$K_{2,x}$	$K_{3,x}$	$F_{bm,x}$
Evaporator	Area	m^2	4.3247	− 0.3030	0.1634	2.9
Turbine	Power output	W_t	2.7051	1.4398	− 0.1776	3.5
Condenser	Area	m^2	4.3247	−0.3030	0.1634	2.9
Pump	Power input	W_p	3.3892	0.0536	0.1538	2.8

$$C_{t,2017} = \frac{C_t \times CEPCI_{2017}}{CEPCI_{2001}} \tag{31}$$

To calculate present value of an annuity, capital recovery factor is used which can be estimated using the following Equation:

$$\text{CRF} = \frac{i(1+i)^T}{(1+i)^T - 1} \tag{32}$$

Where, T denotes total life time of the ORC unit and i denotes interest rate, which corresponds to 5%. LEC of the ORC system can be calculated by the following Equation:

$$\text{LEC} = \frac{\text{CRF} \times C_{t,2017} + C_m}{t_{op} W_{\text{net}}} \tag{33}$$

Where, C_m denotes operation and maintenance cost which is considered as 1.5% of the total cost and top denotes time of operation for a year which is set to 8000 hour.

3 | HEAT TRANSFER SEARCH (HTS) ALGORITHM

Patel et al[52] developed an innovative metaheuristic optimization algorithm namely heat transfer search algorithm. There are three fundamentals mode of heat transfer through which thermal energy is transferred via conduction, convection, and radiation. Any unstable body tends to attain thermal equilibrium using these three modes and tends to get into a stable state with the surroundings. Inspired by the natural phenomenon, the HTS algorithm impersonates the system and surroundings during the accomplishment of thermal equilibrium. It is formulated of three modes namely "conduction phase," "convection phase," and "radiation phase" and equal importance is given to each respective phase of the algorithm.

Similar to a thermodynamic system, molecules and temperature levels of the molecules are imitated as population and design variables in the algorithm. Random population generation is updated in any of the phases and each phase employs equal importance and execution is done using a random number from the generated population. Based on the selection, accepted values of the objective function are updated provided they have enhanced values than the prior. Results are strengthened using updating the solution through individual phase is explained below.

Conduction heat transfer takes place between molecules when two bodies are in physical contact and energy is transferred from molecules with higher energy to molecules with lower energy. In HTS algorithm conduction phase imitates conduction heat transfer and higher and lower energy level molecules are homologous to a population with the higher and lesser objective function value. Solutions are updated by the given formula, for "n" indicates the population size, "m" indicates the design variables, and "g" indicates the number of generation.

$$A'_{j,i} = \begin{cases} A_{k,i} + (-R^2 A_{k,i}), & \text{if } f(A_j) > f(A_k) \\ A_{j,i} + (-R^2 A_{j,i}), & \text{if } f(A_j) < f(A_k) \end{cases} ; \; if \; g \leq g_{\max}/\text{CDF} \tag{33}$$

$$A'_{j,i} = \begin{cases} A_{k,i} + (-r_i A_{k,i}), & \text{if } f(A_j) > f(A_k) \\ A_{j,i} + (-r_i A_{j,i}), & \text{if } f(A_j) < f(A_k) \end{cases}; \; if \; g > g_{\max}/\text{CDF} \tag{34}$$

Where, $A'_{j,i}$ is the updated solution for $j = 1,2,3.....n$ and k is randomly selected solution; i is a randomly selected design variable; g_{max} is the maximum number of generation specified; CDF is conduction factor; R is the probability variable; $R \in [0, 0.33333]$; $r_i \in [0,1]$ is a uniformly distributed random number.

Convection phase imitates convection heat transfer between a system and it is surrounding and body tries to attain thermal equilibrium with the surrounding. In regard to the optimization algorithm, the best solution is surmised to be surrounding and all other solution forms the system. Design variable of the best solution interrelates with the corresponding mean design variable of the population. In convection phase, solutions are updated based on the following equation.

$$A'_{j,i} = A_{j,i} + R(A_s - \text{TCF} \times A_{ms}) \tag{35}$$

$$\text{TCF} = \begin{cases} \text{abs}(R - r_i), & \text{if } g \le g_{\max}/\text{COF} \\ \text{round}(1 + r_i) + (-R^2 A_{j,i}), & if \; g > g_{\max}/\text{COF} \end{cases} \tag{36}$$

Where, COF is the convection factor; R is the probability variable; $R \in [0.6666, 1]$; $r_i \in [0, 1]$ is a uniformly distributed random number; A_s and A_{ms} is the be the temperature of the surrounding and system, respectively; TCF is a temperature change factor.

The radiation phase imitates radiation heat transfer between the system and its surrounding. Similar to another phase, the system interacts with the surrounding to establish a state of thermal steadiness. In this phase, solutions are updated as

$$A'_{j,i} = \begin{cases} A_{j,i} + R(A_{k,i} - A_{j,i}), & \text{if } f(A_j) > f(A_k) \\ A_{j,i} + R(A_{j,i} - A_{k,i}), & \text{if } f(A_j) < f(A_k) \end{cases}; \; if \; g \le g_{\max}/\text{RDF} \tag{37}$$

$$A'_{j,i} = \begin{cases} A_{j,i} + r_i(A_{k,i} - A_{j,i}), & \text{if } f(A_j) > f(A_k) \\ A_{j,i} + r_i(A_{j,i} - A_{k,i}), & \text{if } f(A_j) < f(A_k) \end{cases}; \; if \; g > g_{\max}/\text{RDF} \tag{38}$$

Where RDF is the radiation factor; R is the probability variable; $R \in [0.3333, 0.6666]$; $r_i \in [0, 1]$ is a uniformly distributed random number.

Multi-objective heat transfer search (MOHTS) algorithm renders simultaneous solutions for more than one objective function. MOHTS algorithm incorporates the nondominated solution and save the obtained solutions in an external archive.[53] The MOHTS algorithm uses $\mathcal{E}$-dominance based updating method to check the domination of the solution in the archive. Extended details about MOHTS algorithm is documented in the references.[54-57]

4 | APPLICATION EXAMPLE AND RESULTS DISCUSSION

Study of waste heat recovery system[58] is done in which waste thermal energy from flue gases is recovered using a mixture of nanoparticles and water in the heat exchangers and this energy is

TABLE 3 Operating parameters of ORC system

Parameters	Unit	Value
Heat source temperature	°C	140
Mass flow rate of heat source	kg/s	17.6
Cooling water inlet temperature	°C	20
Mass flow rate of cooling water	kg/s	34.6
Turbine ratio	...	9.5
Turbine efficiency	%	85
Pump efficiency	%	85

Abbreviation: ORC, Organic Rankine Cycle.

imparted to working fluid thus producing power. Continuous fluctuation in the flow rate of flue gases leads to the vacillating study of heat transfer between source fluid and working fluid. Nanofluids after imbibing thermal energy is assumed to achieve a temperature of 140°C and it is considered constant for analysis. Considering the challenges of global warming and ozone depletion, R245fa is used as working fluid and used to expand in the expander to generate mechanical energy. Moreover, its thermodynamic characteristics make it an ideal fluid to be considered for the study. To enhance the heat transfer between heat source fluid and working fluid, CuO and Al_2O_3 nanoparticles are added to water in evaporator and condenser. In the present investigation, nanoparticles are mixed with water and that nanofluid is used for heating and cooling of working fluid in evaporator and condenser. During the heat transfer process, water does not undergo a phase change process and hence nanofluid does not change their phase in evaporator and condenser. Operating parameters for analysis is given in Table 3. Geometric parameters of shell and tube heat exchanger considered for the study are tabulated in Table 4. In this section, results obtained from the single and multiobjective optimization of the system are presented and discussed. Comparative analysis for toward the end of the section, effect of design variables, and effect of turbine ratio, the mass flow rate of heating source fluid and temperature of heating source fluid is discussed.

Initially, single objective optimization is carried out for maximum thermal efficiency and for minimum LEC for CuO and Al_2O_3 based ORC. Design variables for the investigation are mass flow of refrigerant, evaporation pressure, pinch point temperature difference in heat exchangers and concentration of nanoparticles in heat exchangers. The control parameters used for the

TABLE 4 Geometric parameters of shell and tube heat exchanger

Parameter	Evaporator	Condenser
Shell diameter, D_s	0.72 m	0.65 m
Outside diameter of tube, d_o	12.7 mm	12.7 mm
Tube pitch, P_t	$1.25d_o$	$1.3d_o$
Wall thickness, t	1.245 mm	1.651 mm
Tube length, L	2.438 m	2.8 m
Number of passes, N_p	4	3
Number of tubes, N_t	1257	1107
Baffle spacing, B_s	$0.5D_s$	$0.5D_s$

TABLE 5 Range of decision variables

Design variable	Lower bound	Upper bound
Mass flow of refrigerant, kg/s	6	8
Evaporation pressure, kPa	1950	2100
$PPTD_{eva}$, °C	4	10
$PPTD_{cond}$, °C	4	10
Concentration in evaporator ($Ø_{eva}$), %v/v	1	10
Concentration in condenser ($Ø_{cond}$), %v/v	1	10

Abbreviation: PPTD, pinch point temperature difference.

investigation is given in Table 6. Results of single objective optimization show conflicting behavior between two objective functions hence multiobjective optimization is carried out for the nanofluids based system.

4.1 | Multi-objective optimization

In this section, multi-objective optimization using heat transfer search algorithm is carried out and Pareto optimal curve is obtained with the objective of attaining maximum thermal efficiency with minimum LEC. Study of thermo-economic performance of CuO and Al_2O_3 based ORC is done. Bounds of the optimization are given in Table 5. Five optimal points A-E are selected on the Pareto optimal curve and their effect on the objective functions is discussed.

Figure 3 represents Pareto optimal points generated during the multi-objective optimization of CuO and Al_2O_3 based ORC. The results obtained are compared with the Pareto optimal curve of the ORC system operated without nanofluids. Effect of six design variables is studied on thermoeconomic performance of the system. Moreover, the effect of concentration of CuO and Al_2O_3 nanoparticles synthesized with water flowing in heat exchanger is investigated. It was observed from the results that incorporation of nanofluids results in increased thermal efficiency at lower LEC.

For minimum LEC, ORC system operated based on nanofluids yields increased thermal efficiency of 12.49% compared to 12.3% for the conventional system. Reduction of 3.25% in LEC was observed for the system operated with nanofluids resulting in enhanced heat transfer at a lower cost. For the system operated with conventional fluid, variation in thermal efficiency and LEC of 55.28% and 4.03%, respectively, was observed between extreme points of Pareto optimal curve. The

TABLE 6 Control parameters of HTS algorithm

Selection probability of conduction phase	0-0.3333
Selection probability of convection phase	0.3333-0.6666
Selection probability of radiation phase	0.6666-1
Conduction factor	2
Convection factor	10
Radiation factor	2

Abbreviation: HTS, heat transfer search.

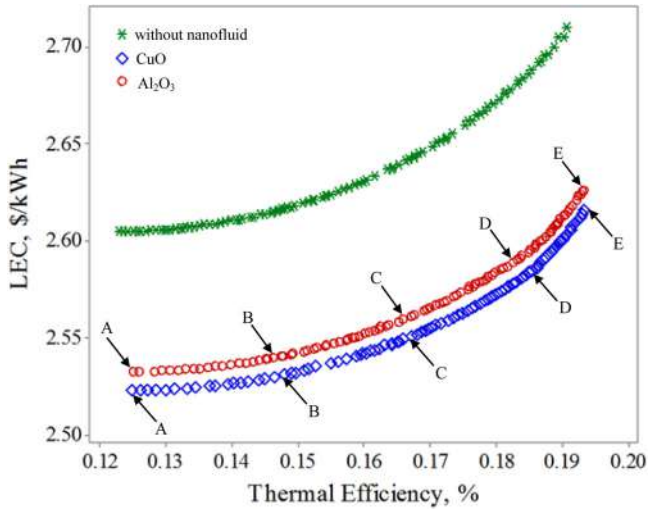

FIGURE 3 Variation of thermal efficiency and levelized energy cost for CuO and Al_2O_3 based ORC. LEC, levelized energy cost; ORC, Organic Rankine Cycle [Color figure can be viewed at wileyonlinelibrary.com]

net power output of 287.18 kW can be obtained from the system operated with conventional fluid at the cost of 2.605 $/kWh. Upon using nanofluids in the system, it was observed that increased power output can be obtained at a lower cost. For a system using CuO nanoparticles, the maximum power output of 289.38 kW can be obtained at cost of 2.523 $/kWh and for system operated with Al_2O_3, maximum output of 288.95 kW can be obtained at 276.04 $/kWh.

The maximum thermal efficiency of 19.3% and 19.32% can be obtained with CuO and Al_2O_3 with 2.616 and 2.62 $/kWh, respectively. From the results, it can be observed that CuO is dominating as compared to Al_2O_3 and gives higher thermal efficiency for reduced LEC. The minimum thermal efficiency of 12.3% can be achieved with LEC of 2.523 $/kWh for CuO and 12.49% can be achieved with 2.53 $/kWh for Al_2O_3. On the Pareto curve, all the optimal point signifies to 10% concentration of nanoparticles in the evaporator for both the case. Whereas the concentration of nanoparticles in condenser has minimum values for maximum thermal efficiency. Values of design variables for five optimal points A-E are given in Table 7.

Pinch point temperature difference in heat exchangers is found to be lower for CuO as compared to Al_2O_3 based cycle. It results in reduced heat transfer surface area of heat exchangers and resembles to lower cost of the system. For optimal points B and C, PPTD for condenser is found to be maximum in CuO compared to Al_2O_3 based cycle. Moreover, it can be observed that PPTD for evaporator increases from point A to E as 5.9697°C to 6.5467°C and for condenser it increases from 6.2918°C to 10°C for Al_2O_3 based ORC. In CuO based ORC, PPTD for evaporator increases from 5.937°C to 6.519°C and for condenser it increases from 6.254°C to 10°C. From the results, it can be concluded that variation in PPTD in the condenser is significant compared to the evaporator to achieve Pareto optimal solution during multi-objective optimization of nanofluids based ORC.

4.2 | Effect of turbine ratio

Figure 4 depicts the effect of turbine ratio on thermal efficiency and LEC of CuO and Al_2O_3 based ORC. Turbine ratio is varied in three steps starting from 9.25, 9.5, and 9.75. With an increase in

TABLE 7 Optimal parameters for design points A-E during multi-objective optimization of CuO and Al_2O_3 based ORC cycle

		Mass flow of refrigerant, kg/s	Evaporation pressure, kPa	$PPTD_{eva}$, °C	$PPTD_{cond}$, °C	Concentration in evaporator, %v/v	Concentration in condenser, %v/v	Thermal efficiency, %	LEC, $/kWh
CuO	A	8	1950.005	5.937	6.254	10	10	0.125	2.523
	B	8	1950.002	6.022	7.455	10	10	0.139	2.526
	C	8	1950.002	6.152	8.730	10	10	0.159	2.541
	D	8	1950.001	6.359	9.601	10	10	0.184	2.582
	E	8	1950	6.519	10	10	1.1	0.193	2.616
Al_2O_3	A	8	1950.0156	5.9697	6.2918	10	10	0.1249	2.5330
	B	8	1950.0294	6.0617	7.9308	10	10	0.1462	2.5400
	C	8	1950.0385	6.1818	9.0726	10	10	0.1659	2.5596
	D	8	1950.0299	6.3585	9.8574	10	9.98	0.1826	2.5890
	E	8	1950	6.5467	10	10	1	0.1932	2.6262

Abbreviations: ORC, Organic Rankine Cycle; PPTD, pinch point temperature difference.

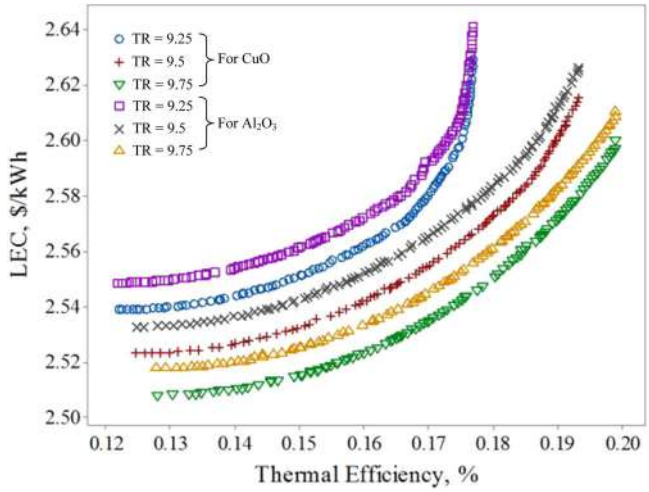

FIGURE 4 Effect of turbine ratio on CuO and Al_2O_3 based ORC during multiobjective optimization. LEC, levelized energy cost; ORC, Organic Rankine Cycle [Color figure can be viewed at wileyonlinelibrary.com]

turbine ratio, thermal efficiency is seen to be increasing and CuO based ORC tends to achieve higher thermal efficiency than Al_2O_3 based cycle because of higher density and higher specific heats of CuO nanofluids. Higher turbine ratio results in lower turbine exit pressure and higher amount of latent heat can be absorbed in the condenser and hence higher thermal efficiency. For turbine ratio 9.25, the optimal curve tends to converge for both the nanoparticles and maximum thermal efficiency of 19.90% is obtained at turbine ratio of 9.75 for Al_2O_3 with the LEC of 2.62 \$/kWh. For Al_2O_3 with an increase in turbine ratio from 9.25 to 9.75, thermal efficiency increases by 12.49% and for CuO it increases by 12.42%. At any given point for specific thermal efficiency, it can be observed that the LEC of CuO based cycle is less than Al_2O_3 based cycle.

4.3 | Effect of heat source temperature

Higher heat source temperature has its significance on the exit temperature of working fluid from the evaporator. The higher temperature of the working fluids yield higher turbine work and eventually at the end of the expansion process, quality of the working fluid will be superheated. It ensures increased life of the turbine blades. Effect of heat source temperature is shown in Figure 5. It can be observed that with an increase in heat source temperature, thermal efficiency increases and LEC reduces because of the higher magnitude of thermal energy being recovered in the heat exchanger. The study is done from three different heat source temperature 135°C, 140°C, and 145°C. However, thermal efficiency is almost same for both the nanofluids as there is little difference in thermal conductivity of CuO and Al_2O_3 which results in almost similar heat transfer between source fluid and working fluid. 19.91% is the maximum thermal efficiency which can be achieved in both the case with the LEC of 2.532 and 2.5403 \$/kWh for CuO and Al_2O_3 based cycle, respectively.

4.4 | Effect of mass flow rate of heat source

Variation in the mass flow rate of working fluid has an effect on heat duty and with an increase in flow rate increased heat transfer can be achieved. Figure 6 represents the effect of mass flow rate on thermal efficiency and LEC of the system and it can be observed that with an increase in mass flow

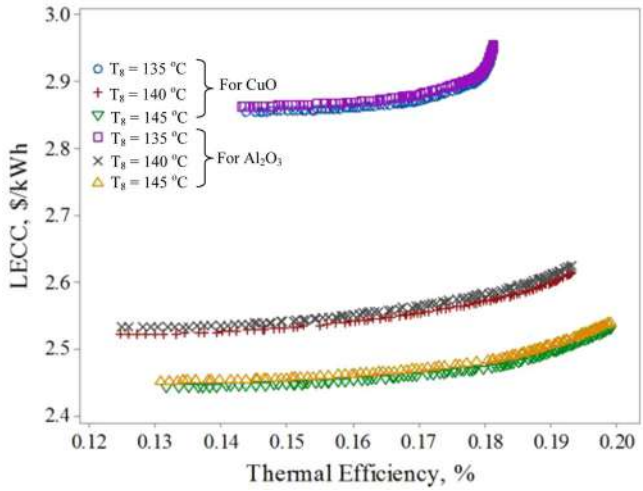

FIGURE 5 Effect of heat source temperature on CuO and Al_2O_3 based ORC during multi-objective optimization. ORC, Organic Rankine Cycle [Color figure can be viewed at wileyonlinelibrary.com]

rate thermal efficiency of the system increases with decrease in LEC. Study of different mass flow rates of heat source is carried out and its value is varied from 17, 17.6, and 18 kg/s. Its effect on LEC is dominant in the case of CuO nanoparticles compared to Al_2O_3 and maximum thermal efficiency of 19.4% and 19.64% can be achieved for CuO and Al_2O_3, respectively. It can be noted that the LEC of Al_2O_3 based cycle is 2.65 $/kWh whereas it is 2.60 $/kWh for CuO based cycle.

4.5 | Effect of design variables

To study the effect of design variables on optimal solutions, sensitivity analysis is carried out for the Pareto points A-E represented on an optimal curve. Figure 7 and Figure 8 represents the effect of design variables for CuO and Al_2O_3 based ORC.

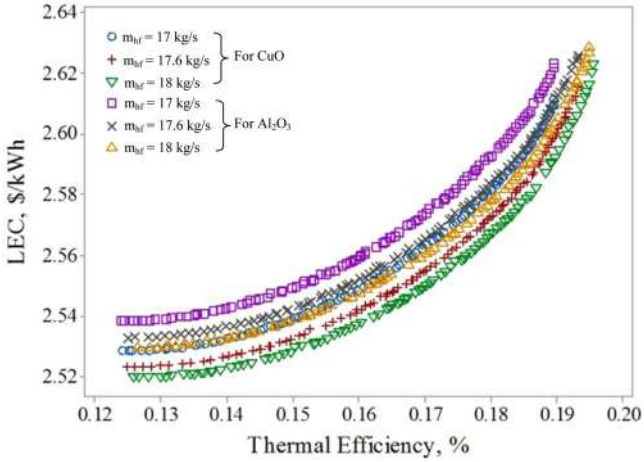

FIGURE 6 Effect of the mass flow rate of heat source fluid on CuO and Al_2O_3 based ORC during multi-objective optimization. ORC, Organic Rankine Cycle [Color figure can be viewed at wileyonlinelibrary.com]

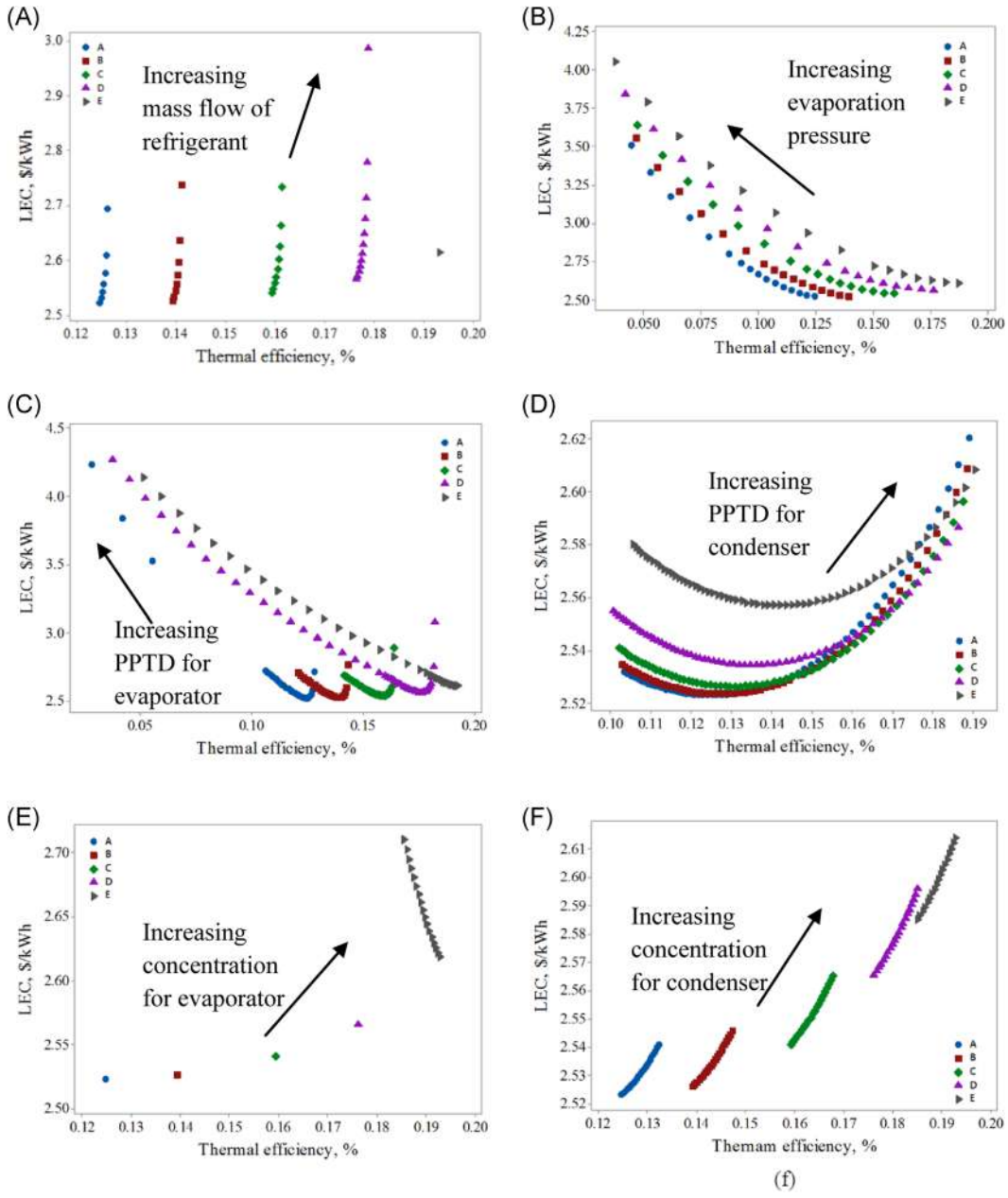

FIGURE 7 Sensitivity of design variables to the optimized value of multi-objective function for CuO based ORC. ORC, Organic Rankine Cycle [Color figure can be viewed at wileyonlinelibrary.com]

Figure 7A and Figure 8B indicate the effect of the mass flow of refrigerant on thermal efficiency and LEC of CuO and Al_2O_3 based ORC, respectively. It can be observed that with an increase in the mass flow rate of refrigerant increase in thermal efficiency increases for both the cycles. With an increase in flow rate, more amount of energy can be absorbed in the evaporator and hence heat rate of the heat exchangers increases which increases the thermal efficiency of the system. Figure 7A and Figure 8B show the effect of evaporation pressure and it can be noted that with increasing pressure thermal efficiency decreases and LEC increases. Effect of

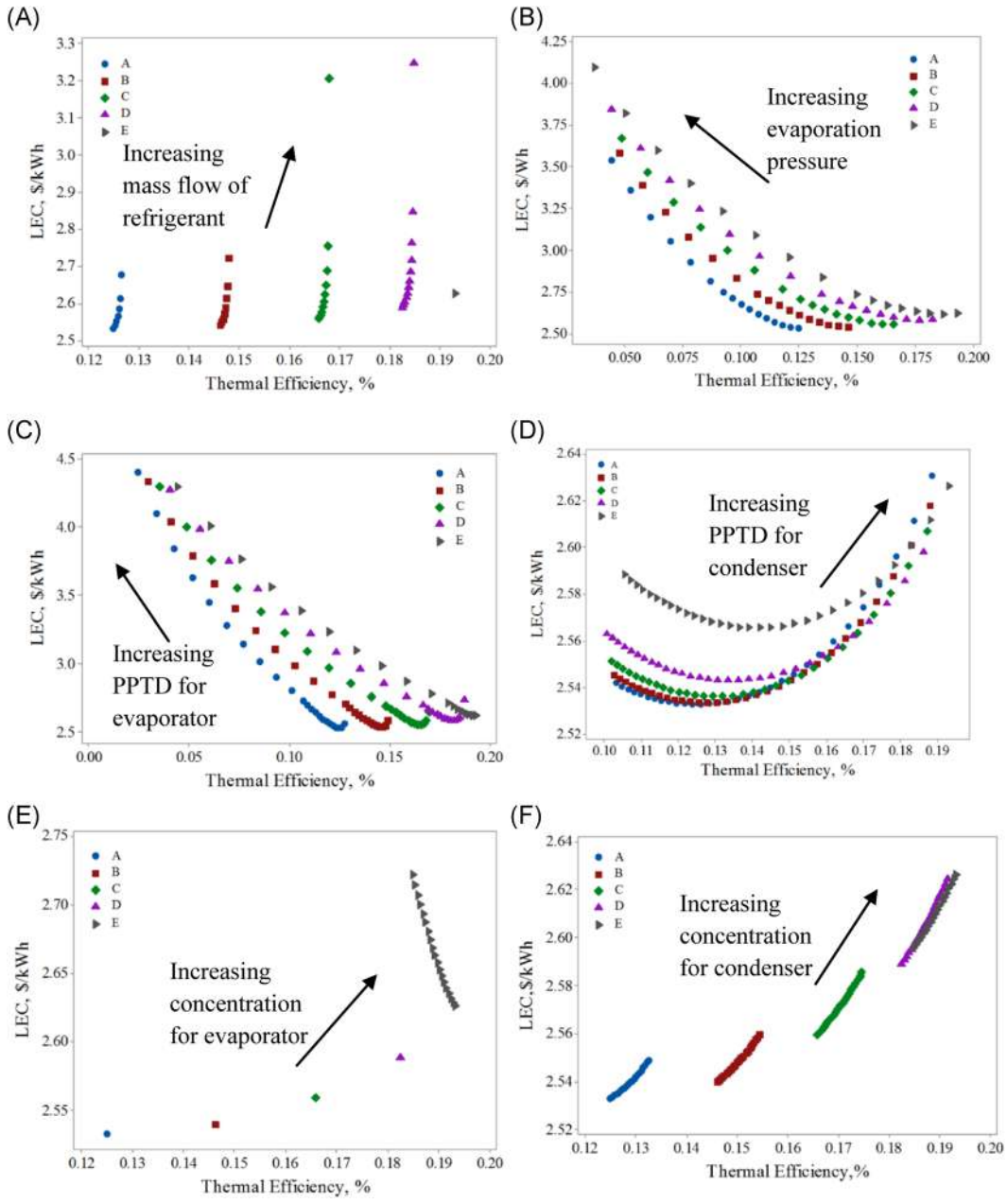

FIGURE 8 The sensitivity of design variables to the optimized value of the multi-objective function for Al_2O_3 based ORC. LEC, levelized energy cost; ORC, Organic Rankine Cycle [Color figure can be viewed at wileyonlinelibrary.com]

evaporation pressure is profound on LEC for higher pressure at point E as compared to lower pressure at point A.

Figure 7C and Figure 8C show the effect of pinch point temperature difference in the evaporator and with increasing temperature difference LEC of the system increases because

higher temperature difference increases the total area of the heat exchanger. Similar behavior can be observed in both CuO and Al_2O_3 based ORC. Moreover, the decrease in thermal efficiency is observed because of decrease heat transfer between source fluid and working fluid.

Effect of pinch point temperature difference in the condenser is shown in Figure 7D and Figure 8D. Thermal efficiency and LEC is found to be decreasing with increasing pinch point temperature difference in the condenser and after an optimum point, there is a steep increase in LEC as compared to thermal efficiency. Heat rejection has a dominant effect on first law efficiency of the system as compared to heat absorbed in the heat exchanger.

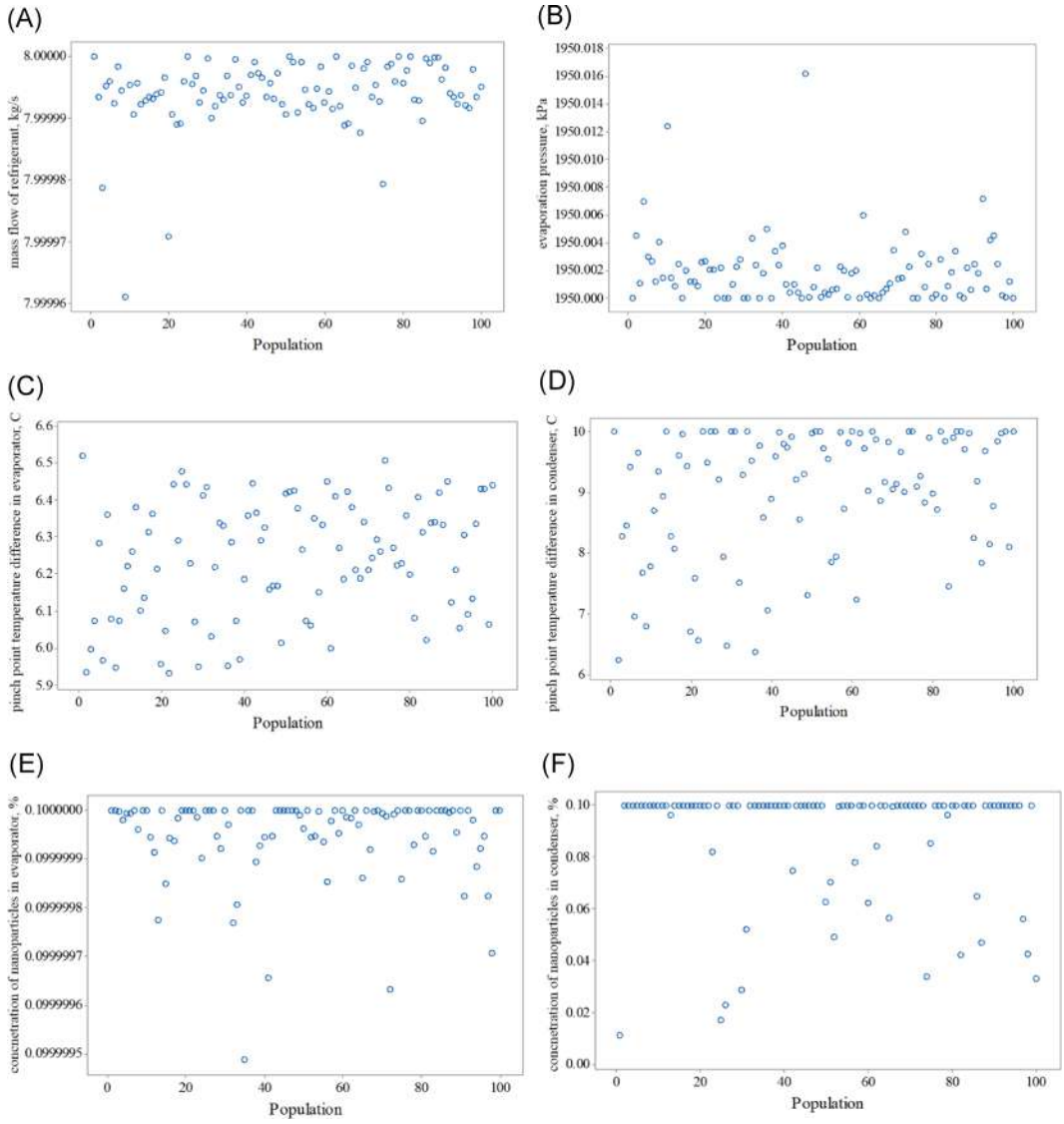

FIGURE 9 Distribution of design variables during multi-objective optimization of CuO based ORC (A) mass flow rate of refrigerant (B) evaporation pressure (C) pinch point temperature difference for evaporator (D) pinch point temperature difference for condenser (E) concentration of nanoparticles for evaporator (F) concentration of nanoparticles for the condenser. LEC, levelized energy cost; ORC, Organic Rankine Cycle; PPTD, pinch point temperature difference [Color figure can be viewed at wileyonlinelibrary.com]

Figure 7E and Figure 8E depict the effect of concentration of nanoparticles in the evaporator and it can be observed that very few solution points are obtained by changing the concentration of CuO and Al_2O_3 in the evaporator. This situation originate because of constraint infringement with variation in values of design variables and hence optimized values are very sensitive.

Effect of concentration of nanoparticles in the condenser is represented in Figure 7E and Figure 8E. It shows with increasing concentration, thermal efficiency, and LEC increases. However, increasing concentration of Al_2O_3 in condenser has a negligible increase in thermal efficiency is observed at higher concentrations from point D to E. Effect of concentration of nanoparticles in condenser has a profound effect on thermal efficiency as compared to the evaporator.

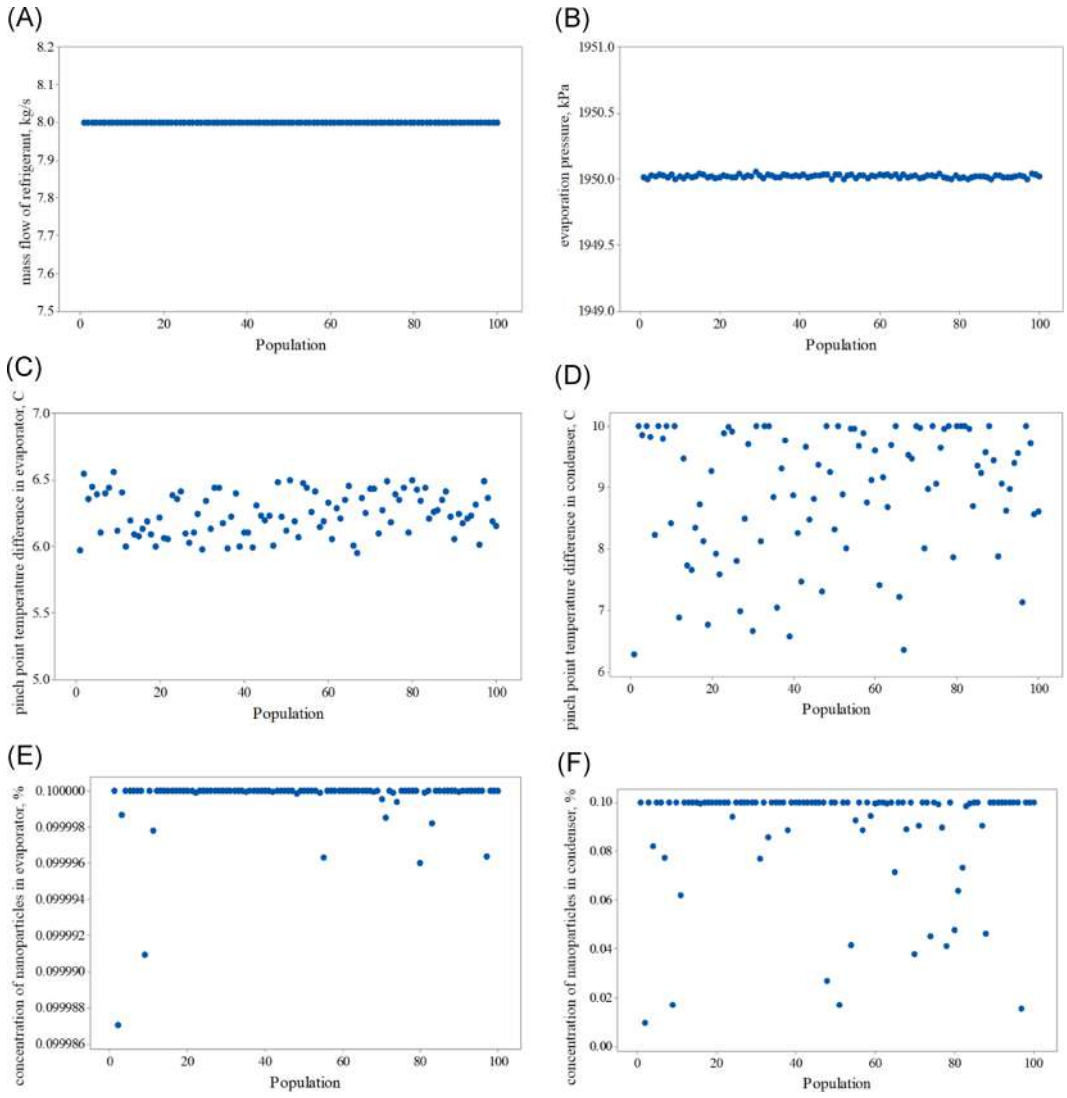

FIGURE 10 Distribution of design variables during multi-objective optimization of Al_2O_3 based ORC (A) mass flow rate of refrigerant (B) evaporation pressure (C) pinch point temperature difference for evaporator (D) pinch point temperature difference for condenser (E) concentration of nanoparticles for evaporator (F) concentration of nanoparticles for the condenser. ORC, Organic Rankine Cycle [Color figure can be viewed at wileyonlinelibrary.com]

4.6 | Distribution of design variables

Figure 9 and Figure 10 shows the population distribution of design variables corresponding to design variables. It can be observed that the effect of the mass flow of refrigerant, evaporation pressure, and concentration of nanoparticles in the evaporator is invariable for CuO and Al_2O_3 based ORC. Scattered distribution is seen for the variables pinch point temperature difference in heat exchangers and in the concentration of nanoparticles for the condenser. These variables play a significant role in achieving optimal solution between thermal efficiency and LEC of the system. Pinch point temperature difference in condenser shows most diversified distribution among all the optimal solutions of design variables.

5 | CONCLUSION

This paper addresses thermoeconomic optimization of nanofluids based ORC for recovering heat energy from exhaust flue gases. Working fluid used in the system is R245fa and CuO and Al_2O_3 nanoparticles are considered for the investigation. It can be observed that heat exchangers operated with nanofluid results in increased waste heat recovery and enhanced thermal performance.

- Overall, 35.2% variation in thermal efficiency is observed at the cost of 3.5% variation in LEC between extreme design points of Pareto front for Al_2O_3, and CuO based ORC.
- Further, for any given value of the thermal efficiency, lower LEC is observed with CuO based ORC as compared to Al_2O_3 based ORC.
- The effect of turbine ratio, mass flow rate of heat source fluid and temperature of heat source is investigated and reported. With the increase in the turbine ratio, LEC of ORC is reduced for a given value of thermal efficiency.
- Likewise, the increase in heat source temperature as well as the mass flow rate of heat source fluid also reduces the LEC of ORC at the given value of thermal efficiency.
- Distribution of each design variables corresponding to Pareto optimal solution points of Al_2O_3 and CuO based is also presented.
- Pinch point temperature difference for heat exchangers and concentration of nanoparticles in condenser shows a profound effect on the optimal design of the system during thermo-economic optimization.

NOMENCLATURE

A	area (m^2)
a	particle radius (m)
A_{cs}	cross flow area (m^2)
B	baffle spacing (m)
C_p	specific heat at constant pressure (J/kgK)
C_{bm}	bare module cost ($)
C_t	total cost ($)
C_m	maintenance cost ($)
CP	purchase cost ($)

D_s shell diameter (m)
d_o outside diameter of tube (m)
d_i inside diameter of tube (m)
D_e equivalent diameter (m)
F friction factor
F_{bm} bare module cost factor
h specific enthalpy (J/kg)
h_{fS} heat transfer coefficient of shell side (W/m^2K)
h_{fT} heat transfer coefficient of tube side (W/m^2K)
K thermal conductivity (W/mk)
K_{wall} thermal conductivity of wall of heat exchanger (W/mK)
L length of tube (m)
N_t number of tubes
Nu Nusselt number
P_t tube pitch (m)
Pr Prandtl number
Q heat load (W)
Re Reynolds number
t_{op} time of operation (hrs)
U_o overall heat transfer coefficient (W/m^2K)
U_m mean velocity (m/s)
W_{net} net work output (W)
$\dot{m}$ mass flow rate (kg/s)
$\dot{V}$ volume flow rate (m^3/s)

GREEK LETTERS

ρ density (kg/m^3)
μ viscosity ($N.s/m^2$)
$\emptyset$ concentration

SUBSCRIPTS

np nanoparticles
l liquid
f base fluid
eff effective
nf nanofluid
sp single phase
tp two phase
eva evaporator
cond condenser
t total

ORCID

Vivek K. Patel http://orcid.org/0000-0001-7508-186X

REFERENCES

1. Feng Y, Zhang Y, Li B, Yang J, Shi Y. Comparison between regenerative organic Rankine cycle (RORC) and basic organic Rankine cycle (BORC) based on thermoeconomic multi-objective optimization considering exergy efficiency and levelized energy cost (LEC). *Energy Convers Manage*. 2015;96:58-71.
2. Chen H, Goswami DY, Stefanakos EK. A review of thermodynamic cycles and working fluids for the conversion of low-grade heat. *Renewable Sustainable Energy Rev*. 2010;14(9):3059-67.
3. Etemoglu AB. Thermodynamic investigation of low-temperature industrial waste-heat recovery in combined heat and power generation systems. *Int Commun Heat Mass Transfer*. 2013;42:82-88.
4. Li M, Wang J, He W, et al. Construction and preliminary test of a low-temperature regenerative Organic Rankine Cycle (ORC) using R123. *Renewable Energy*. 2013;57:216-22.
5. Kang SH. Design and experimental study of ORC (organic Rankine cycle) and radial turbine using R245fa working fluid. *Energy*. 2012;41(1):514-24.
6. Li M, Wang J, He W, Wang B, Ma S, Dai Y. Experimental evaluation of the regenerative and basic organic Rankine cycles for low-grade heat source utilization. *J Energy Eng*. 2013;139(3):190-197.
7. Clemente S, Micheli D, Reini M, Taccani R. (2011) Simulation model of an experimental small-scale ORC cogenerator. *Proceedings of the First International Seminar on ORC Power Systems*, 22-23. Delft, The Netherlands.
8. Imran M, Park BS, Kim HJ, Lee DH, Usman M, Heo M. Thermo-economic optimization of regenerative Organic Rankine cycle for waste heat recovery applications. *Energy Convers Manage*. 2014;87:107-118.
9. Wang ZQ, Zhou NJ, Guo J, Wang XY. Fluid selection and parametric optimization of organic Rankine cycle using low temperature waste heat. *Energy*. 2012;40(1):107-115.
10. Liu BT, Chien KH, Wang CC. Effect of working fluids on organic Rankine cycle for waste heat recovery. *Energy*. 2004;29(8):1207-1217.
11. Hung TC. Waste heat recovery of organic Rankine cycle using dry fluids. *Energy Convers Manage*. 2001;42(5):539-553.
12. Hajabdollahi Z, Hajabdollahi F, Tehrani M, Hajabdollahi H. Thermo-economic environmental optimization of Organic Rankine Cycle for diesel waste heat recovery. *Energy*. 2013;63:142-151.
13. Wang J, Yan Z, Wang M, Li M, Dai Y. Multi-objective optimization of an organic Rankine cycle (ORC) for low grade waste heat recovery using evolutionary algorithm. *Energy Convers Manage*. 2013;71:146-158.
14. Scardigno D, Fanelli E, Viggiano A, Braccio G, Magi V. A genetic optimization of a hybrid organic Rankine plant for solar and low-grade energy sources. *Energy*. 2015;91:807-815.
15. Fu BR, Lee YR, Hsieh JC. Design, construction, and preliminary results of a 250-kW organic Rankine cycle system. *Appl Therm Eng*. 2015;80:339-346.
16. Han S, Seo J, Choi BS. Development of a 200 kW ORC radial turbine for waste heat recovery. *J Mech Sci Technol*. 2014;28(12):5231-5241.
17. Manjili FE, Dehghani H, Shamekhi L. Parametric analysis of dry hydrocarbons on the performance of organic Rankine cycle improved by working fluid reheating. *Heat Transf-Asian Res*. 2015;44(8):738-752.
18. Sarkar J. Property-based selection criteria of low GWP working fluids for organic Rankine cycle. *J Brazilian Soc Mech Sci Eng*. 2017;39(4):1419-1428.
19. Desai NB, Bandyopadhyay S. Thermo-economic analysis and selection of working fluid for solar organic Rankine cycle. *Appl Therm Eng*. 2016;95:471-481.
20. Zhang C, Fu J, Kang J, Fu W. Performance optimization of low-temperature geothermal organic Rankine cycles using axial turbine isentropic efficiency correlation. *J Brazilian Soc Mech Sci Eng*. 2018;40(2):61.
21. Desai NB, Bandyopadhyay S. Thermo-economic comparisons between solar steam Rankine and organic Rankine cycles. *Appl Therm Eng*. 2016;105:862-875.
22. Kakaç S, Pramuanjaroenkij A. Review of convective heat transfer enhancement with nanofluids. *Int J Heat Mass Transfer*. 2009;52(13-14):3187-3196.
23. Trisaksri V, Wongwises S. Critical review of heat transfer characteristics of nanofluids. *Renewable Sustainable Energy Rev*. 2007;11(3):512-523.
24. Devendiran DK, Amirtham VA. A review on preparation, characterization, properties and applications of nanofluids. *Renewable Sustainable Energy Rev*. 2016;60:21-40.

25. Nallusamy S. "Thermal conductivity analysis and characterization of copper oxide nanofluids through different techniques". *J Nano Res*. 2016;40:102-112.
26. Shima PD, Philip J, Raj B. Influence of aggregation on thermal conductivity in stable and unstable nanofluids. *Appl Phys Lett*. 2010;97:1531131-1531133. https://doi.org/10.1063/1.3497280
27. Hejazian M, Moraveji MK. A comparative analysis of single and two-phase models of turbulent convective heat transfer in a tube for TiO_2 nanofluid with CFD. *Numerical Heat Transfer, Part A: Applications*. 2013;63(10):795-806.
28. Xuan Y, Li Q. Investigation on convective heat transfer and flow features of nanofluids. *J Heat Transfer*. 2003;125(1):151-155.
29. Yang Y, et al. Heat transfer properties of nanoparticle-in-fluid dispersions (nanofluids) in laminar flow. *Int J Heat Mass Transfer*. 2005;48(6):1107-1116.
30. Farajollahi B, Etemad SG, Hojjat M. Heat transfer of nanofluids in a shell and tube heat exchanger. *Int J Heat Mass Transfer*. 2010;53(1-3):12-17.
31. Wang X, Xu X, Choi SUS. Thermal conductivity of nanoparticle-fluid mixture. *J Thermophys Heat Transfer*. 1999;13(4):474-480.
32. Nallusamy S. Characterization of Al2O3/water nanofluid through shell and tube heat exchangers over parallel and counter flow. *J Nano Res*. 2017;45:155-163.
33. Pak BC, Cho YI. Hydrodynamic and heat transfer study of dispersed fluids with submicron metallic oxide particles. *Experimental Heat Transfer an International Journal*. 1998;11(2):151-170.
34. O'Hanley H, Boungiorno J, McKrell T, Hu L-W. (2011). Measurement and model correlation of specific heat capacity of water-based nanofluids with silica, alumina and copper oxide nanoparticles. *In ASME 2011 International Mechanical Engineering Congress and Exposition. American Society of Mechanical Engineers*, Denver, CO.
35. Dai Y, Wang J, Gao L. Parametric optimization and comparative study of organic Rankine cycle (ORC) for low grade waste heat recovery. *Energy Convers Manage*. 2009;50(3):576-582.
36. Roy J, Mishra M, Misra A. Parametric optimization and performance analysis of a waste heat recovery system using Organic Rankine Cycle. *Energy*. 2010;35(12):5049-5062.
37. Shengjun Z, Huaixin W, Tao G. Performance comparison and parametric optimization of subcritical Organic Rankine Cycle (ORC) and transcritical power cycle system for low-temperature geothermal power generation. *Appl Energy*. 2011;88(8):2740-2754.
38. Xi H, et al. Parametric optimization of regenerative organic Rankine cycle (ORC) for low grade waste heat recovery using genetic algorithm. *Energy*. 2013;58:473-482.
39. Wang J, et al. Multi-objective optimization design of condenser in an organic Rankine cycle for low grade waste heat recovery using evolutionary algorithm. *Int Commun Heat Mass Transfer*. 2013;45:47-54.
40. Zhang X, et al. Multi-objective optimization and fast decision-making method for working fluid selection in organic Rankine cycle with low-temperature waste heat source in industry. *Energy Convers Manage*. 2018;172:200-211.
41. Turgut MS, Turgut OE. Multi-objective optimization of the basic and single-stage Organic Rankine Cycles utilizing a low-grade heat source. *Heat Mass Transf*. 2018;55(2):353-374.
42. Feng Y, et al. Performance comparison of low-grade ORCs (organic Rankine cycles) using R245fa, pentane and their mixtures based on the thermoeconomic multi-objective optimization and decision makings. *Energy*. 2015;93:2018-2029.
43. Bergman TL, et al. *Fundamentals of heat and mass transfer*. Hoboken, NJ: John Wiley & Sons; 2011.
44. Brinkman H. The viscosity of concentrated suspensions and solutions. *J Chem Phys*. 1952;20(4):571-571.
45. Kakac S, Liu H, Pramuanjaroenkij A. *Heat exchangers: selection, rating, and thermal design*. Boca Raton, FL: CRC press; 2002.
46. Leong K, Saidur R, Mahlia TMI, Hau YH. Modeling of shell and tube heat recovery exchanger operated with nanofluid based coolants. *Int J Heat Mass Transfer*. 2012;55(4):808-816.
47. Leong K, Yang C, Murshed S. A model for the thermal conductivity of nanofluids–the effect of interfacial layer. *J Nanopart Res*. 2006;8(2):245-254.
48. Shah RK, Sekulic DP. Fundamentals of heat exchanger design. Hoboken, NJ: John Wiley & Sons; 2003.

49. Xuan Y, Roetzel W. Conceptions for heat transfer correlation of nanofluids. *Int J Heat Mass Transfer*. 2000;43(19):3701-3707.
50. Akilu S, et al. A review of thermophysical properties of water based composite nanofluids. *Renewable Sustainable Energy Rev*. 2016;66:654-678.
51. Gherasim I, et al. Experimental investigation of nanofluids in confined laminar radial flows. *Int J Therm Sci*. 2009;48(8):1486-1493.
52. Patel VK, Savsani VJ. Heat transfer search (HTS): a novel optimization algorithm. *Inf Sci (Ny)*. 2015;324:217-246.
53. Patel V, Savsani V, Mudgal A. Efficiency, thrust, and fuel consumption optimization of a subsonic/sonic turbojet engine. *Energy*. 2018;144:992-1002.
54. Raja BD, Jhala R, Patel V. Multi-objective thermo-economic and thermodynamics optimization of a plate–fin heat exchanger. *Heat Transf—Asian Res*. 2018;47:253-270.
55. Raja BD, Jhala R, Patel V. Many-objective optimization of cross-flow plate-fin heat exchanger. *Int J Therm Sci*. 2017;118:320-339.
56. Raja BD, Jhala R, Patel V. Many-objective optimization of shell and tube heat exchanger. *Therm Sci Eng Prog*. 2017;2:87-101.
57. Raja BD, Jhala R, Patel V. Thermal-hydraulic optimization of plate heat exchanger: A multi-objective approach. *Int J Therm Sci*. 2018;124:522-535.
58. Sung, T, Yun E, Kim HD, et al. Performance characteristics of a 200-kW organic Rankine cycle system in a steel processing plant. *Appl Energy*. 2016;183:623-635.

How to cite this article: Prajapati PP, Patel VK. Comparative analysis of nanofluid based organic Rankine cycle through thermo-economic optimization. *Heat Transfer—Asian Res*. 2019;1-26. https://doi.org/10.1002/htj.21528